FXa cleaves the SARS-CoV-2 spike protein and blocks cell entry to protect against infection with inferior effects in B.1.1.7 variant — **Source link** ↗

Jianhua Yu, Wenjuan Dong, Jing Wang, Lei Tian ...+10 more authors

Institutions: City of Hope National Medical Center, Northern Arizona University, University of New Mexico, Washington University in St. Louis

Topics: Viral entry and Furin

Related papers:

- Hydroxychloroquine-mediated inhibition of SARS-CoV-2 entry is attenuated by TMPRSS2.

- Rationally Designed ACE2-Derived Peptides Inhibit SARS-CoV-2.

- Human Surfactant Protein D Binds Spike Protein and Acts as an Entry Inhibitor of SARS-CoV-2 Pseudotyped Viral Particles

- Structure-based phylogeny identifies avoralstat as a TMPRSS2 inhibitor that prevents SARS-CoV-2 infection in mice.

- SARS-CoV-2 spike protein binding selectively accelerates substrate-specific catalytic activity of ACE2.

1 **FXa cleaves the SARS-CoV-2 spike protein and blocks cell entry to protect against**

2 **infection with inferior effects in B.1.1.7 variant**

3 Wenjuan Dong[1,2,†] , Jing Wang[1,2, †], Lei Tian[1,2, †], Jianying Zhang[3], Heather Mead[4], Sierra A.

4 Jaramillo[4], Aimin Li[5], Ross E. Zumwalt[6], Sean P.J. Whelan[7], Erik W. Settles[4], Paul S. Keim[4],

5 Bridget Marie Barker[4], Michael A. Caligiuri[1,2,8*], and Jianhua Yu[1,2,8,9,*]

6 [1]Department of Hematology & Hematopoietic Cell Transplantation, City of Hope National

7 Medical Center, Los Angeles, CA 91010, USA

8 [2]Hematologic Malignancies Research Institute, City of Hope National Medical Center, Los

9 Angeles, CA 91010, USA

10 [3]Department of Computational and Quantitative Medicine, City of Hope National Medical Center,

11 Los Angeles, CA 91010, USA

12 [4]Pathogen and Microbiome Institute, Northern Arizona University, Flagstaff, AZ 86011, USA

13 [5]Pathology Core of Shared Resources Core, Beckman Research Institute, City of Hope National
14 Medical Center, Los Angeles, CA 91010, USA

15 [6] Department of Pathology, University of New Mexico, Albuquerque, NM 87131, USA

16 [7]Department of Molecular Microbiology, Washington University School of Medicine, St. Louis,

17 MO 63110, USA

18 [8]City of Hope Comprehensive Cancer Center, Los Angeles, CA 91010, USA

19 [9] Department of Immuno-Oncology, City of Hope, Los Angeles, CA 91010, USA

20 [†]These authors contributed equally

21 [*]Correspondence should be addressed to Jianhua Yu, PhD, jiayu@coh.org; Michael A. Caligiuri,

22 MD, mcaligiuri@coh.org

23

24 **Short title: FXa cuts spike and blocks COVID-19**

25

26

27

28

29 **Abstract**

30 **The ongoing coronavirus disease 2019 (COVID-19) pandemic is caused by infection with**

31 **severe acute respiratory syndrome coronavirus 2 (SARS-CoV-2). Human natural defense**

32 **mechanisms against SARS-CoV-2 are largely unknown. Serine proteases (SPs) including**

33 **furin and TMPRSS2 cleave SARS-CoV-2 spike protein, facilitating viral entry. Here, we**

34 **show that FXa, a SP for blood coagulation, is upregulated in COVID-19 patients compared**

35 **to non-COVID-19 donors and exerts anti-viral activity. Mechanistically, FXa cleaves the**

36 **SARS-CoV-2 spike protein, which prevents its binding to ACE2, and thus blocks viral entry.**

37 **Furthermore, the variant B.1.1.7 with several mutations is dramatically resistant to the anti-**

38 **viral effect of FXa compared to wild-type SARA-CoV-2 *in vivo* and *in vitro*. The anti-**

39 **coagulant rivaroxaban directly inhibits FXa and facilitates viral entry, whereas the indirect**

40 **inhibitor fondaparinux does not. In a lethal humanized hACE2 mouse model of SARS-CoV-**

41 **2, FXa prolonged survival while combination with rivaroxaban but not fondaparinux**

42 **abrogated this protection. These preclinical results identify a previously unknown SP**

43 **function and associated anti-viral host defense mechanism and suggest caution in**

44 **considering direct inhibitors for prevention or treatment of thrombotic complications in**

45 **COVID-19 patients.**

46

47 **Introduction**

48 SARS-CoV-2 is the pathogen responsible for the global COVID-19 pandemic[1]. To date, over

49 170,000,000 cases and approximately 3,500,000 deaths have been recorded with a worldwide

50 mortality rate of 2%[2]. The public health and economic consequences have been devastating.

51 Although some strategies such as neutralizing antibodies and vaccines are being developed or

52 testing in the clinic, the pandemic rages on with new concerns regarding the emergence of resistant

53 strains[3-6].

54 Angiotensin-converting enzyme 2 (ACE2) has been identified as the host receptor for SARS-CoV-

55 2[7,8]. SARS-CoV-2 uses its spike (S) protein to bind to ACE2 and enter host cells. Several host

56 serine proteases (SPs) have been identified as facilitating SARS-CoV-2 entry via cleavage of its S

57 protein into functional S1 and S2 subunits[9,10]. Furin cuts the S protein at the PRRAR (R-R-A-R685

58 ↓) site into S1 and S2 subunits at virus budding, while TMPRSS2 cleaves at the S2' site (P-S-K-

2

59   R815 ↓) at virus entry, and both cleavages enhance efficiency of SARS-CoV-2 infection[9,11].

60   Another SP family member, coagulation factor Xa (FXa) binds to tissue factor to initiate

61   conversion of prothrombin to thrombin in the clotting cascade[12]. The direct FXa inhibitors

62   rivaroxaban, apixaban, and edoxaban, and betrixaban as well as the indirect inhibitor fondaparinux

63   have been developed as clinical anti-coagulants[13], and several direct inhibitors are currently being

64   evaluated for use in patients at high-risk for COVID-19[14].

65

66   Here we show that FXa inhibits SARS-CoV-2 entry. Mechanistically, FXa binds to and cleaves S

67   protein, which produced a different cleavage pattern than that of furin and TMPRSS2, and blocked

68   S protein binding to ACE2. The effect was pronounced for the ancestral wild type variant, but was

69   diminished in the B.1.1.7 variant. Exogenous FXa protected mice from lethal infection in a

70   humanized hACE2 mouse model of COVID-19 using the wild type variant but not the B.1.1.7

71   variant. The anti-viral effect of FXa was attenuated by the direct FXa inhibitor rivaroxaban (RIVA)

72   but not the indirect inhibitor fondaparinux (FONDA) both *in vivo* and *in vitro*.

73

74   **Results**

75   To identify changes in SPs during SARS-CoV-2 infection, we examined their expression in lung

76   samples from COVID-19 patients using an immunohistochemistry assay (IHC). Due to the lack of

77   specific antibodies directly against FXa, we detected FX expression since ~100% FX can be

78   activated to FXa at injury sites when platelets are exposed to both collagen and thrombin[15]. Our

79   IHC analysis indicated that thrombin was highly expressed in lungs from COVID-19 patients

80   compared to that from non-COVID-19 patients (Extended Data Fig. 1a), consistent with previous

81   data[16,17]. We found FX was significantly increased in the lungs of COVID-19 patients compared

82   to non-COVID-19 donors; in contrast, we did not observe consistent upregulation of other tested

83   SPs (Fig. 1a and Extended Data Fig. 1b). We found that FX was also increased in the liver

84   (Extended Data Fig. 1c) and serum, which is the source and carrier of FXa, in COVID-19 patients

85   compared to non-COVID-19 donors (Fig. 1, b and c).

86   To investigate the consequences of increased FXa during SARS-CoV-2 infection, we cloned FXa

87   into the pCDH-mCherry vector and assessed its function using the vesicular stomatitis virus

88   (VSV)-SARS-CoV-2 chimeric virus[18]. 293T cells were co-transfected with ACE2 and FXa or

89   control empty vector (EV). After 24 hours, cells were infected by VSV-SARS-CoV-2. The

90   percentage of infected cells (GFP positive cells) was examined at the indicated time points using

91   flow cytometry. Surprisingly, at indicated hours post infection (hpi), compared to EV transfected

92   group, the percentage of infected cells was decreased in FXa transfected group, indicating that the

93   presence of FXa efficiently blocked viral infection (Fig. 1d). SARS-CoV-2 infection depends not

94   only on ACE2 but also TMPRSS2[10]. When 293T cells were co-transfected with FXa, ACE2, and

95   TMPRSS2, FXa again blocked viral infection, showing a more pronounced effect during the early

96   time points in the presence of TMPRSS2 (Fig. 1e). To confirm our results, we generated an MA104

97   epithelial kidney cell line stably expressing FXa (MA104-FXa) (Extended Data Fig. 2a). The cells

98   were infected by VSV-SARS-CoV-2 at different MOIs and the infectivity was determined at 16-

99   48 hpi. We found that MA104-FXa cells showed markedly decreased infection at each time point

100 and at all MOIs compared to MA104-EV control cells (Fig. 1f and Extended Data Fig. 2b). The

101 viral titers of the supernatant from the infected MA104-FXa cells at 24 and 48 hpi were

102 significantly decreased compared to that from MA104-EV cells, suggesting over-expressing FXa

103 also impaired viral production (Extended Data Fig. 2c and d). We also compared the role of FXa

104 with other SPs in viral infection of parental MA104 cells. Unlike pretreatment with furin,

105 TMPRSS2, or trypsin, all of which increased VSV-SARS-CoV-2 infection, pre-treatment with

106 FXa inhibited viral infection (Extended Data Fig. 3a and b). Consistent with this, the viral titer of

107 the supernatant from FXa-treated MA104 cells infected with VSV-SARS-CoV-2 was significantly

108 decreased, while the viral titer of infected cells treated with furin, TMPRSS2 or trypsin increased,

109 compared to infected cells treated with vehicle control (PBS) (Extended Data Fig. 3c).

110 Furthermore, to determine if FXa blocks viral infection by targeting SARS-CoV-2 or host cells,

111 we first constructed an FXa-Fc fusion protein expression plasmid and purified the protein from

112 Chinese hamster ovary (CHO) cells. Then, we co-incubated VSV-SARS-CoV-2 with or without

113 FXa-Fc fusion protein *in vitro* for 1 hour before adding the mixture into MA104 cells. The rate of

114 infection was examined at the indicated timepoints. We found that pre-incubation of VSV-SARS-

115 CoV-2 with FXa-Fc fusion protein significantly inhibited viral infection in a dose-dependent

116 manner (from 62.5 pM to 1μM), suggesting that FXa could block viral infection by targeting

117 SARS-CoV-2 (Fig. 1, g, h, and Extended Data Fig. 4). Of note, the inactivated FXa had no effect

118 on viral infection (Extended Data Fig. 4). To determine the effects of FXa on viral production, we

119 infected the MA104 cells with VSV-SARS-CoV-2 at a very low MOI (0.001) and with FXa protein

120   at the indicated concentrations. We found that the viral titer showed a dose-dependent decrease

121   with the increase of FXa protein, suggesting that FXa plays an essential role in inhibiting viral

122   production (Extended Data Fig. 5a). To determine whether FXa also inhibits viral infection

123   through interaction with host cells, we preincubated FXa-Fc fusion protein with MA104 cells for

124   1 hour and then washed out the medium before infecting cells with VSV-SARS-CoV-2. We found

125   that FXa-Fc fusion protein pre-treatment with the MA104 cells did not significantly affect viral

126   infection (Extended Data Fig. 5b and c). We next used live SARS-CoV-2 to infect Vero E6 and

127   MA104-EV cells followed by quantitative assessment of viral load using an immuno-plaque assay.

128   We found that pre-incubation FXa with live SARS-CoV-2 prior to infection significantly reduced

129   viral infection in both Vero E6 and MA104 cells compared to buffer control, consistent with the

130   above VSV-SARS-CoV-2 chimeric virus data (Fig. 1, i and j). The anti-viral effect of FXa against

131   live SARS-CoV-2 infection was also confirmed with a traditional plaque assay with Vero E6 cells

132   (Extended Data Fig. 5d). Together, our results showed that FXa, a serine protease that is

133   upregulated following SARS-CoV-2 infection in host cells, inhibited viral infection and thus

134   possessed an anti-viral activity, in distinct contrast to other serine proteases such as furin and

135   TMPRSS2.

136   To study the mechanism(s) of the anti-viral activity of FXa, we compared the binding between

137   FXa and various subunits of SARS-CoV-2 S protein. We found that FXa had the strongest binding

138   affinity toward the full-length S protein and to a lesser extent to subunit S1, subunit S2 and the

139   receptor binding domain (RBD) compared to the control Fc protein (Fig. 2a). Pull-down assay

140   showed that FXa but not the Fc control protein co-precipitated with S protein (Fig. 2b). We then

141   measured the binding affinity of FXa and the full-length S protein. The results showed that the

142   binding affinity of FXa to S protein is in the nanogram range (Fig. 2c). These results suggest that

143   FXa binds to the S protein, which might inhibit viral entry efficiency. Virus entry is followed by

144   important conformational changes of viral proteins via cleavage of the S protein by host SPs. To

145   determine whether FXa could cleave S protein, we incubated full-length S protein with FXa,

146   followed by immunoblotting. Furin and TMPRSS2 served as positive controls, as they are known

147   to induce functional conformational changes of S protein. We found that full-length S was cut into

148   three fragments by FXa with the size of approximately 60 KD, then 50 KD and 29 KD (Fig. 2d),

149   consistent with *in silico* prediction of two FXa cleavage sites on S protein, Ile-(Asp/Glu)-Gly-Arg

150   (R1000) and Gly-Arg (R567) (Fig. 2e). This cleavage pattern was in contrast to that of furin and

151   TMPRSS2, which both cut full-length S protein into the ~80 KD subunit S1. Cleavage by FXa did

152   not produce the ~80 KD subunit S1.

153   Given that FXa could cut S protein into different sizes, we used ELISA to determine whether

154   cleavage by FXa affected binding of the S protein to ACE2. The ELISA data indicated that S

155   protein pre-treated with FXa resulted in decreased binding affinity to ACE2 (Fig. 3a). Flow

156   cytometry further confirmed this result, demonstrate that FXa-pre-treated S protein could not

157   efficiently bind to ACE2-expressing HEK293T cells (Fig. 3, b and c). We also showed that FXa

158   still bound to S protein when S protein was already bound to ACE2 (Fig. 3, d, e and f), yet FXa

159   still cleaved the S protein bound to ACE2 (Extended Data Fig. 6). Overall, our results indicate that

160   FXa could be an efficient inhibitor of viral entry via its interaction with S protein.

161   An emergent SARS-CoV-2 strain has been found to substitute aspartic acid–614 for glycine

162   (D614G) in the S protein[19]. Thus, we tested whether FXa had similar functional interactions with

163   the D614G S protein. FXa could still bind with and cleave the D614G S protein (Extended Data

164   Fig. 7a-c), and the binding affinity between ACE2 and D614G S protein decreased if S protein

165   was pretreated with FXa (Extended Data Fig. 7d and e).

166   COVID-19 patients with an increased risk of thrombosis are treated with direct FXa inhibitors

167   (e.g., rivaroxaban) or indirect inhibitors (e.g., fondaparinux)[14,20]. We therefore asked if

168   rivaroxaban (RIVA) or fondaparinux (FONDA) affect the anti-viral activity of FXa. Neither

169   RIVA nor FONDA blocked the binding of FXa to S protein (Fig. 3g), and neither drug alone had

170   any effect on VSV-SARS-CoV-2 infectivity; however, the direct FXa inhibitor RIVA blocked

171   FXa-induced anti-viral activity, whereas the indirect FXa inhibitor FONDA did not (Fig. 3, h and

172   i). We measured viral titers in the supernatants collected from this inhibitor experiment, which

173   confirmed that RIVA but not FONDA significantly reduced FXa-induced anti-viral activity

174   (Extended Data Fig. 8a). Furthermore, cleavage assay showed that the direct FXa inhibitor RIVA

175   but not the indirect inhibitor FONDA inhibited cleavage of S protein by FXa (Fig. 3j). Consistent

176   with this, pretreatment of the mixture of S protein and FXa with RIVA or FONDA, followed by

177   incubation with ACE2, showed that RIVA but not FONDA significantly diminished the effect of

178   FXa on inhibiting the binding of S protein to ACE2 as demonstrated by ELISA, presumably by

179   inhibiting cleavage of S protein by RIVA but not by FONDA (Fig. 3k). The ELISA results in

180   Figure 3k were validated by flow cytometry analysis (Fig. 3l and Extended Data Fig. 8b). Our data

181   indicate that the direct rather than indirect inhibitor of FXa could diminish FXa-mediated blockade

182   of viral entry by inhibiting the cleavage of S protein by FXa so that intact S protein can efficiently

183   bind to ACE2. We repeated these experiments with live SARS-CoV-2 and MA104 cells

184   demonstrating identical results (Fig. 3m).

185   To evaluate the potential effect of FXa *in vivo*, we used humanized K18-hACE2 mice as an

186   infection model of SARS-CoV-2[21,22] and inoculated them with 3×10^5 pfu SARS-CoV-2, followed

187   by intranasal administration of the FXa-Fc protein or two controls, saline and the Fc protein. The

188   body weight of the mice was monitored. We found that the majority of mice in the untreated and

189   Fc-treated groups exhibited a dramatic decrease in their body weight at day 5 and were euthanized

190   at that time or shortly thereafter, while three of the five mice treated with FXa-Fc started the

191   recovery of their body weight at day 7 (Fig. 4a). The FXa-Fc treated group lived significantly

192   longer than the two control groups, with no difference between the control groups (Fig. 4b). We

193   isolated RNA and used quantitative real-time PCR to measure the viral load in trachea, lung, and

194   brain tissues. Viral load in the FXa-Fc treated group was approximately 1,000-fold lower than that

195   of the two control groups, indicating that FXa-Fc significantly restricted SARS-CoV-2 infection

196   *in vivo* (Fig. 4, c, d, and e). Consistent with this, IHC showed that expression of viral nucleocapsid

197   protein (NP) was also markedly decreased in the brain and lung tissues from the FXa-Fc treated

198   group compared to the untreated and Fc-treated group (Fig. 4f). The histological study showed that

199   FXa-Fc-treated mice had more intact lung structure and less pathological damage compared to the

200   two control groups (Fig. 4f). To evaluate the effects of the two types of FXa inhibitors, the direct

201   inhibitor RIVA and the indirect inhibitor FONDA *in vivo*, we were administrated into FXa-treated

202   (intranasally) SARS-CoV-2-infected mice. Consistent with the *in vitro* data, we found that direct

203   FXa inhibitor RIVA significantly blocked the anti-viral and survival advantage afforded by

204   intranasal administration of FXa-Fc, while the indirect FXa inhibitor FONDA had no significant

205   effect on the anti-viral and survival advantage afforded by intranasal administration of FXa-Fc

206   alone (Fig. 5, a-e). These *in vivo* results with live SARS-CoV-2 provide preclinical support for

207   the use of an indirect FXa inhibitor such as FONDA as an anti-coagulant when preventing or

208   treating thrombotic complications of COVID-19, while avoiding the use of a direct FXa inhibitor

209   such as the anti-coagulant RIVA under similar clinical circumstances.

210   A variant of SARS-CoV-2 (known as B.1.1.7), which was emerged with a large number of

211   mutations, may be associated with an increased transmissibility and risk of death compared with

212   other variants[23,24]. By analyzing the S protein sequence of the B.1.1.7 variant, we found there is a

213   nonsynonymous mutation A570D in the S protein close to the predicted FXa cleavage site. In order

214   to evaluate the effect of the anti-viral function of FXa on the variant, we infected the Vero E6 and

215   MA104 cells with the original emergent SARS-CoV-2 (wild-type; WT) or B.1.1.7 virus pretreated

216   with different concentrations of FXa. The immuno-plaque results showed that the anti-viral effect

217   of FXa was significantly and dramatically decreased against B.1.1.7 variant infection compared to

218   the WT infection (Fig. 6a). Furthermore, the results were confirmed by viral infection with various

219   MOIs, which showed that FXa could still block WT infection even at a very high MOI (MOI=8),

220   but had little effect on B.1.1.7 infection blockade at the same MOI (Fig. 6b). To figure out the

221   mechanism of this difference, we detected the binding affinity between FXa and WT S protein or

222   B.1.1.7 S protein. Both ELISA and flow cytometry results showed that FXa had a significantly

223   lower binding affinity with B.1.1.7 S protein compared to that with WT S protein (Fig. 6, c and d),

224   indicating that the mutants on B.1.1.7 S protein blocked FXa anti-viral effect by affecting the

225   binding affinity of FXa to the S protein. We also tested the effects of the direct and indirect FXa

226   inhibitors in the B.1.1.7 variant infection using the WT strain as control. We found that RIVA

227   could efficiently block the anti-viral effect of FXa in a dose-dependent manner starting as low as

228   0.05 µg/ml dose, while FONDA did not even at the high dose of 50 µg/ml, against the B.1.1.7

229   variant infection in both Vero E6 and MA104 hosts (Extended Data Fig. 9a and b). These data

230   were validated in similar experiments with gradient concentrations of FXa in both Vero E6 and

231   MA104 hosts (Extended Data Fig. 10 and 11).

232   Next, we compared the anti-viral effect of FXa against WT and B.1.1.7 infection *in vivo*.

233   Consistent with the *in vitro* data, we found that the anti-viral and survival advantage afforded by

234   FXa-Fc was abolished or significantly decreased in the B.1.1.7 variant-infected group compared

235   to the WT-infected group (Fig. 7, a-d). Collectively, our data demonstrate that the variant B.1.1.7

236   strain with a mutated spike protein was resistant to the FXa inhibition *in vitro* and *in vivo* compared

237   to the WT strain, which might explain the higher transmission[25-27] and mortality[28] rates for this

238   dangerous variant of concern.

239

240

Discussion

Here we identify a novel mechanism of human host anti-viral defense involving FXa at the time of SARS-CoV-2 infection, which binds to and cleaves viral S protein, blocking viral entry into host cells. Exogenous administration of FXa reduced viral load and protected a humanized hACE2 mouse model of COVID-19 from lethal infection, an effect that was attenuated by a direct but not indirect FXa inhibitor and anti-coagulant, which has implications for clinical therapeutic responses.

SARS-CoV-2 is a newly emergent human pathogen that utilizes the ACE2 receptor to enter host cells. Proteolytic processing S protein by SPs such TMPRSS2, furin, and trypsin enhances the binding affinity between host ACE2 and the processed S protein[10]. In the course of infection, unlike the immune tolerance exhibited by bats, in human SARS-CoV-2 at times excessively activates the inflammatory components of the immune system of humans leading to the cytokine release syndrome [29], which can be fatal in some, yet non-existent in others with the same exposure [30]. Therefore, identification of the body's natural defense mechanisms against SARS-CoV-2 is important for developing effective prevention as well as therapeutic strategies. Our report here of a natural defense mechanism involving the binding to and cleavage of the SARS-CoV-2 S protein by FXa, effectively blocking viral entry into host cells, may lead to the development of such strategies. Like TMPRSS2 and furin, FXa belongs to the family of SPs that each cleave S protein, but have different cleavage targets and subsequent effects on viral entry into host cells. TMPRSS2 and furin cleave the S protein at the S1/S2 site of at RRAR (685R), followed by the S2' site KPSKR (R856), resulting in priming the SARS-CoV-2 fusion step. How the FXa cleavage of the S protein blocks entry of SARS-CoV-2 into host cells is currently unknown. But our *in silico* modeling, which is supported by experimental evidence, indicates that the cleavage sites of FXa on S protein are at Ile-(Asp/Glu)-Gly-Arg (R1000) or Gly-Arg (R567), distinct from the S1/S2 or the S2' site. This likely results in a unique conformational change of the S protein when forming a syncytium[31]. The most conserved region of the RBD is between amino acids 306 to 527, which is close to the FXa cleavage site (R567)[8]. As such, the cleavage by FXa near the RBD may adversely impact the conserved conformation of the RBD. The S protein is a type 1 viral fusion protein with two conserved heptad repeat regions, HR-N (916-950) and HR-C (1150-1185), which may form a 6-helix bundle allowing for a better fusion between the viral and host cell membranes[32,33]. The two

9

271 likely cleavage sites of FXa are located within the HR-N and the HR-C repeat and could impair

272 the formation of a hetero-stranded complex, impairing the fusion process.

273 The B.1.1.7 variant of concern emerged in the United Kingdom in September 2020 and has

274 demonstrated higher transmissibility[25-27] and mortality[28]. It has been shown that some vaccines

275 and neutralizing antibodies have lower efficacy from B.1.1.7 variant infection than WT strain

276 infection[34-38]. However, the reason for its poor outcomes remained elusive[39]. Our description of

277 the previously unknown FXa barrier to SARS-COV-2 infection and its differential effect on the

278 B.1.1.7 variant is a possible, or at least partial, explanation. Our data showed that the variant

279 B.1.1.7 strain with a mutated spike protein was resistant to the FXa inhibition *in vitro* and *in vivo*

280 compared to the WT strain. Therefore, the host anti-viral defense system depending on FXa maybe

281 not strong enough to protect people from B.1.1.7 variant infection. The basis for the variant

282 differential could be the A570D mutation, which only emerged as a dominant change in the B.1.1.7

283 variant near the FXa cleavage site. FXa showed a significantly lower binding affinity with B.1.1.7

284 S protein compared to that with WT S protein, which might be affected by the A570D mutation in

285 the B.1.1.7 S protein. But the spike protein structure is complex and dynamic, which means more

286 distal differences could also play a role.

287 FXa is required for the conversion of prothrombin to thrombin in the clotting cascade[12], and may

288 have a role in inflammation[40]. Both of these processes are dysregulated in some patients with

289 COVID-19[30,41]. Although it is likely that the viral defense mechanism that we have described here

290 is active and important in controlling SARS-CoV-2 infection in asymptomatic and mildly

291 symptomatic individuals, the endogenous overexpression of FXa during serious SARS-CoV-2

292 infection may also contribute to the pathogenesis and complications of COVID-19, especially the

293 thrombotic events[41,42]. Therefore, the use of FXa as a therapeutic agent is straightforward. There

294 could be at least two alternative pathways forward in considering FXa as a therapeutic agent for

295 severe SARS-CoV-2 infection. The first would be to co-administer an indirect FXa inhibitor as an

296 anti-coagulant in combination with the FXa-Fc fusion protein described in this report or with a

297 recombinant FXa, because we show that the indirect FXa inhibitor fondaparinux does not interfere

298 with FXa's cleavage of S protein or its therapeutic effect against the live virus *in vivo*. The second

299 approach would be to modify the chemical structure of FXa such that its enzymatic activity for

300 cleavage of the S protein is retained while that of prothrombin conversion is lost. This latter

301 approach might also be considered as a preventative approach for individuals who are not

10

302   vaccinated and are highly susceptible to severe COVID-19 or those same individuals who are

303   vaccinated yet fail to develop effective immunity to SARS-CoV-2.

304   There are four clinically approved direct FXa inhibitors, including rivaroxaban, apixaban,

305   edoxaban as well as betrixaban) and one indirect FXa inhibitor fondaparinux for use as anti-

306   thrombotic agents in patients with hypercoagulable states[43]. Our study showed that in the presence

307   of a direct inhibitor of FXa, rivaroxaban, the anti-SARS-CoV-2 activity of FXa is affected not by

308   the binding of the S protein but by the cleavage of the S protein. Further, rivaroxaban completely

309   abrogates the decrease in viral load and the protective effect against lethal SARS-CoV-2 infection

310   conferred by exogenous FXa. Our study suggests that the use of direct FXa inhibitors such as

311   rivaroxaban, in patients highly susceptible for severe COVID-19 as is currently being evaluated in

312   a number of studies[14], should likely proceed with caution as it is at least conceivable from our

313   work that such studies could result in an increase in viral load. Importantly, the FXa indirect

314   inhibitor , fondaparinux, which we found to not block the protective effects of FXa against SARS-

315   CoV-2, has been found to be safe and efficacious for venous thrombosis prophylaxis in

316   hospitalized COVID-19 patients[20].

317   The factors responsible for predicting clinical outcomes in patients stricken with COVID-19

318   remain incomplete[44]. Here we show that the precursor FX of FXa is upregulated in COVID-19

319   patients. We identify a new mechanism of anti-viral defense in human and prove its importance

320   in a transgenic animal model that mimics the human disease. Our work would suggest that future

321   studies should examine the quality and quantity of FXa enzymatic activity against the SARS-CoV-

322   2 S protein to determine if it can improve our understanding of who may be most susceptible to

323   SARS-CoV-2 infection and who might be treated with an FXa indirect anti-coagulant inhibitor.

324

325

REFERENCES

1   Hu, B., Guo, H., Zhou, P. & Shi, Z. L. Characteristics of SARS-CoV-2 and COVID-19. *Nat Rev Microbiol*, doi:10.1038/s41579-020-00459-7 (2020).

2   Worldometer.   *Worldometer's   COVID-19   data.*, https://www.worldometers.info/coronavirus/country/us/ (2020).

3   Polack, F. P. *et al.* Safety and Efficacy of the BNT162b2 mRNA Covid-19 Vaccine. *N Engl J Med* **383**, 2603-2615, doi:10.1056/NEJMoa2034577 (2020).

4   Li, W. *et al.* High Potency of a Bivalent Human VH Domain in SARS-CoV-2 Animal Models. *Cell* **183**, 429-441 e416, doi:10.1016/j.cell.2020.09.007 (2020).

5   Shi, R. *et al.* A human neutralizing antibody targets the receptor-binding site of SARS-CoV-2. *Nature* **584**, 120-124, doi:10.1038/s41586-020-2381-y (2020).

6   Dai, L. *et al.* A Universal Design of Betacoronavirus Vaccines against COVID-19, MERS, and SARS. *Cell* **182**, 722-733 e711, doi:10.1016/j.cell.2020.06.035 (2020).

7   Meyerowitz, E. A., Richterman, A., Gandhi, R. T. & Sax, P. E. Transmission of SARS-CoV-2: A Review of Viral, Host, and Environmental Factors. *Ann Intern Med*, doi:10.7326/M20-5008 (2020).

8   Wang, Q. *et al.* Structural and Functional Basis of SARS-CoV-2 Entry by Using Human ACE2. *Cell* **181**, 894-904 e899, doi:10.1016/j.cell.2020.03.045 (2020).

9   Hoffmann, M., Kleine-Weber, H. & Pohlmann, S. A Multibasic Cleavage Site in the Spike Protein of SARS-CoV-2 Is Essential for Infection of Human Lung Cells. *Mol Cell* **78**, 779-784 e775, doi:10.1016/j.molcel.2020.04.022 (2020).

10   Hoffmann, M. *et al.* SARS-CoV-2 Cell Entry Depends on ACE2 and TMPRSS2 and Is Blocked by a Clinically Proven Protease Inhibitor. *Cell* **181**, 271-280 e278, doi:10.1016/j.cell.2020.02.052 (2020).

11   Bestle, D. *et al.* TMPRSS2 and furin are both essential for proteolytic activation of SARS-CoV-2 in human airway cells. *Life Sci Alliance* **3**, doi:10.26508/lsa.202000786 (2020).

12   Golino, P. *et al.* Involvement of tissue factor pathway inhibitor in the coronary circulation of patients with acute coronary syndromes. *Circulation* **108**, 2864-2869, doi:10.1161/01.CIR.0000105900.21445.3D (2003).

13   Lu, G. *et al.* A specific antidote for reversal of anticoagulation by direct and indirect inhibitors of coagulation factor Xa. *Nat Med* **19**, 446-451, doi:10.1038/nm.3102 (2013).

14   Al-Horani, R. A. Potential Therapeutic Roles for Direct Factor Xa Inhibitors in Coronavirus Infections. *Am J Cardiovasc Drugs* **20**, 525-533, doi:10.1007/s40256-020-00438-6 (2020).

15   Koklic, T., Majumder, R., Weinreb, G. E. & Lentz, B. R. Factor XA binding to phosphatidylserine-containing membranes produces an inactive membrane-bound dimer. *Biophys J* **97**, 2232-2241, doi:10.1016/j.bpj.2009.07.043 (2009).

16   Chen, J., Wu, H., Yu, Y. & Tang, N. Pulmonary alveolar regeneration in adult COVID-19 patients. *Cell Res* **30**, 708-710, doi:10.1038/s41422-020-0369-7 (2020).

17   George, P. M., Wells, A. U. & Jenkins, R. G. Pulmonary fibrosis and COVID-19: the potential role for antifibrotic therapy. *Lancet Respir Med* **8**, 807-815, doi:10.1016/S2213-2600(20)30225-3 (2020).

18   Zang, R. *et al.* Cholesterol 25-hydroxylase suppresses SARS-CoV-2 replication by blocking membrane fusion. *Proc Natl Acad Sci U S A* **117**, 32105-32113, doi:10.1073/pnas.2012197117 (2020).

19   Korber, B. *et al.* Tracking Changes in SARS-CoV-2 Spike: Evidence that D614G Increases Infectivity of the COVID-19 Virus. *Cell* **182**, 812-827 e819, doi:10.1016/j.cell.2020.06.043 (2020).

12

372 20   Russo, V. *et al.* Thromboprofilaxys With Fondaparinux vs. Enoxaparin in Hospitalized COVID-19
373   Patients: A Multicenter Italian Observational Study. *Front Med (Lausanne)* **7**, 569567,
374   doi:10.3389/fmed.2020.569567 (2020).
375 21   Oladunni, F. S. *et al.* Lethality of SARS-CoV-2 infection in K18 human angiotensin-converting
376   enzyme 2 transgenic mice. *Nature communications* **11**, 6122, doi:10.1038/s41467-020-19891-7
377   (2020).
378 22   Dong, W. *et al.* The K18-hACE2 Transgenic Mouse Model Recapitulates Non-Severe and Severe
379   COVID-19 in Response to Infectious Dose of SARS-CoV-2 Virus. 2021.2005.2008.443244,
380   doi:10.1101/2021.05.08.443244 %J bioRxiv (2021).
381 23   Volz, E. *et al.* Assessing transmissibility of SARS-CoV-2 lineage B.1.1.7 in England. *Nature* **593**, 266-
382   269, doi:10.1038/s41586-021-03470-x (2021).
383 24   Davies, N. G. *et al.* Increased mortality in community-tested cases of SARS-CoV-2 lineage B.1.1.7.
384   *Nature* **593**, 270-274, doi:10.1038/s41586-021-03426-1 (2021).
385 25   Volz, E. *et al.* Assessing transmissibility of SARS-CoV-2 lineage B.1.1.7 in England. *Nature*,
386   doi:10.1038/s41586-021-03470-x (2021).
387 26   Davies, N. G. *et al.* Increased mortality in community-tested cases of SARS-CoV-2 lineage B.1.1.7.
388   *Nature*, doi:10.1038/s41586-021-03426-1 (2021).
389 27   Davies, N. G. *et al.* Estimated transmissibility and impact of SARS-CoV-2 lineage B.1.1.7 in England.
390   *Science*, doi:10.1126/science.abg3055 (2021).
391 28   Grint, D. J. *et al.* Case fatality risk of the SARS-CoV-2 variant of concern B.1.1.7 in England, 16
392   November to 5 February. *Euro Surveill* **26**, doi:10.2807/1560-7917.ES.2021.26.11.2100256 (2021).
393 29   Irving, A. T., Ahn, M., Goh, G., Anderson, D. E. & Wang, L. F. Lessons from the host defences of
394   bats, a unique viral reservoir. *Nature* **589**, 363-370, doi:10.1038/s41586-020-03128-0 (2021).
395 30   Jose, R. J. & Manuel, A. COVID-19 cytokine storm: the interplay between inflammation and
396   coagulation. *Lancet Respir Med* **8**, e46-e47, doi:10.1016/S2213-2600(20)30216-2 (2020).
397 31   Jaimes, J. A., Millet, J. K. & Whittaker, G. R. Proteolytic Cleavage of the SARS-CoV-2 Spike Protein
398   and the Role of the Novel S1/S2 Site. *iScience* **23**, 101212, doi:10.1016/j.isci.2020.101212 (2020).
399 32   Xia, S. *et al.* Fusion mechanism of 2019-nCoV and fusion inhibitors targeting HR1 domain in spike
400   protein. *Cell Mol Immunol* **17**, 765-767, doi:10.1038/s41423-020-0374-2 (2020).
401 33   Huang, Y., Yang, C., Xu, X. F., Xu, W. & Liu, S. W. Structural and functional properties of SARS-CoV-
402   2 spike protein: potential antivirus drug development for COVID-19. *Acta Pharmacol Sin* **41**, 1141-
403   1149, doi:10.1038/s41401-020-0485-4 (2020).
404 34   Wu, K. *et al.* Serum Neutralizing Activity Elicited by mRNA-1273 Vaccine. *N Engl J Med*,
405   doi:10.1056/NEJMc2102179 (2021).
406 35   Collier, D. A. *et al.* Sensitivity of SARS-CoV-2 B.1.1.7 to mRNA vaccine-elicited antibodies. *Nature*,
407   doi:10.1038/s41586-021-03412-7 (2021).
408 36   Edara, V. V. *et al.* Infection and mRNA-1273 vaccine antibodies neutralize SARS-CoV-2 UK variant.
409   *medRxiv*, doi:10.1101/2021.02.02.21250799 (2021).
410 37   Wang, P. *et al.* Antibody resistance of SARS-CoV-2 variants B.1.351 and B.1.1.7. *Nature*,
411   doi:10.1038/s41586-021-03398-2 (2021).
412 38   Shen, X. *et al.* SARS-CoV-2 variant B.1.1.7 is susceptible to neutralizing antibodies elicited by
413   ancestral spike vaccines. *Cell Host Microbe*, doi:10.1016/j.chom.2021.03.002 (2021).
414 39   Plante, J. A., B. M. Mitchell, K. S. Plante, K. Debbink, S. C. Weaver, V. D. Menachery. The variant
415   gambit: COVID-19's   next   move.   *Cell   Host   Microbe*   **29**,
416   doi:https://doi.org/10.1016/j.chom.2021.02.020 (2021).
417 40   Bukowska, A. *et al.* Coagulation factor Xa induces an inflammatory signalling by activation of
418   protease-activated receptors in human atrial tissue. *Eur J Pharmacol* **718**, 114-123,
419   doi:10.1016/j.ejphar.2013.09.006 (2013).

420 41   Al-Samkari, H. *et al.* COVID-19 and coagulation: bleeding and thrombotic manifestations of SARS-
421   CoV-2 infection. *Blood* **136**, 489-500, doi:10.1182/blood.2020006520 (2020).
422 42   Wichmann, D. *et al.* Autopsy Findings and Venous Thromboembolism in Patients With COVID-19:
423   A Prospective Cohort Study. *Ann Intern Med* **173**, 268-277, doi:10.7326/M20-2003 (2020).
424 43   Rupprecht, H. J. & Blank, R. Clinical pharmacology of direct and indirect factor Xa inhibitors. *Drugs*
425   **70**, 2153-2170, doi:10.2165/11538030-000000000-00000 (2010).
426 44   Richardson, S. *et al.* Presenting Characteristics, Comorbidities, and Outcomes Among 5700
427   Patients Hospitalized With COVID-19 in the New York City Area. *JAMA* **323**, 2052-2059,
428   doi:10.1001/jama.2020.6775 (2020).

429

430 **Methods**

431 **Patient sample collection**

432 Patients were collected and tested positive for SARS-CoV-2 at City of Hope. Autopsy samples

433 were provided by Dr. Ross Zumwalt at the University of New Mexico School of Medicine. The

434 concentration of FXa in the serum of patient samples was measured using ELISA (LS-F10420-1,

435 LSBIO). The protocols for human specimen collection were approved by the institutional review

436 board of City of Hope.

437 **Cells**

438 Monkey kidney epithelial-derived MA104 cells were maintained in medium 199 supplemented

439 with 10% FBS, penicillin (100 U/ml), and streptomycin (100 μg/ml). To overexpress FXa in

440 MA104 cells, the cells were infected with lentivirus encoding FXa to generate MA104-FXa cells.

441 Monkey kidney epithelium-derived Vero cells, Vero E6 cells, human embryonic kidney-derived

442 HEK293T cells, and Chinese hamster ovary (CHO) cells were cultured in DMEM with 10% FBS,

443 penicillin (100 U/ml), and streptomycin (100 μg/ml). All cell lines were routinely tested to confirm

444 absence of mycoplasma using the MycoAlert Plus Mycoplasma Detection Kit from Lonza

445 (Walkersville, MD).

446 **VSV-SARS-CoV-2 infection**

447 The VSV-SARS-CoV-2 chimeric virus expressing GFP was kindly provided by Sean Whelan at

448 Washington University School of Medicine. The virus is decorated with SARS-CoV-2 S protein

449 in place of the native glycoprotein (G) [1] . For VSV-SARS-CoV-2 infection, MA104 cells were

450 seeded 24 hours before the infection at a confluency of 70% in a 96-well plate. VSV-SARS-CoV-

451 2 virus and varying amounts (12.5 μg/ml, 25 μg/ml, 50 μg/ml, and 100 μg/ml) of the FXa-Fc

14

452   fusion protein were co-incubated at 37°C for 1 hour and then were added to the cells. To assess

453   the effect of FXa inhibitors, FXa protein was preincubated with or without 50 µg/ml rivaroxaban

454   or fondaparinux separately for 1 hour at room temperature. Infectivity was assessed by detecting

455   GFP fluorescence using a Zeiss fluorescence microscope (AXIO observer 7) and/or determined by

456   the percentage of GFP(+) cells analyzed using a Fortessa X20 flow cytometer (BD Biosciences)

457   at 16, 24, 36, and 48 hours post infection (hpi). To determine viral production, Vero cells were

458   pre-seeded for 24 hours and infected with the supernatants collected from MA104 cells infected

459   by VSV-SARS-CoV at 24 or 48 hpi. The supernatants were diluted by 5-fold before the viral

460   production assay.

Generation and purification of FXa

462   CHO cells were transduced with a pCDH lentiviral vector expressing FXa to produce the FXa-Fc

463   fusion protein for functionality assays. For this purpose, FXa fused with human IgG4 was

464   reconstructed as previously reported [2]. mCherry was co-expressed with FXa for FACS-sorting to

465   purify transduced cells using a FACS Aria II cell sorter (BD Biosciences, San Jose, CA, USA).

466   Conditional supernatants from lentivirus-infected CHO cells sorted by FACS were used to purify

467   the FXa-Fc fusion protein using a protein G column (89927, Thermo Fisher). For *in vivo* testing,

468   the protein G column-purified FXa-Fc fusion protein was desalted using fast protein liquid

469   chromatography (FPLC).

SARS-CoV-2 neutralization, cell infection, plaque assay, and immunoplaque assay

471   The following reagent was obtained through BEI Resources, NIAID, NIH: SARS-Related

472   Coronavirus 2, Isolate USA-WA1/2020, NR-52281 (wild-type, WT) and SARS-Related

473   Coronavirus 2, Isolate USA/CA_CDC_5574/2020, NR-54011 (B.1.1.7). Virus isolates were

474   passaged in Vero E6 cells (ATCC CRL-1586) as previously described[3]. Virus concentration was

475   determined using immunoplaque assay (also called focus forming assay) [4]. For the plaque assay,

476   120 pfu SARS-CoV-2 was incubated with diluted sera for 2 hours at 37 °C. Then Vero E6 cells

477   were infected with 250 µl virus-sera mixture for 1 hour. After infection, the medium containing

478   virus was removed, and overlay medium containing FBS-free DMEM and 2% low-melting point

479   agarose was added. At 72 hours post infection, infected cells were fixed by 4% paraformaldehyde

480   (PFA) overnight, and stained with 0.2% crystal violet. For the immunoplaque assay, 100 pfu of

481   live SARS-CoV-2 variants were incubated with diluted sera for 1 hour and then the virus antibody

482 mixture was added to Vero E6 cells for 1 hour at 37℃. After 1 hour the virus containing medium

483 was removed, overlayed with medium containing methylcellulose and 2% FBS DMEM, and

484 incubated at 37℃. At 24 hours after infection, infected cells were fixed by 4% paraformaldehyde

485 for 20 minutes at room temperature and then permeabilized by 0.5% Triton X-100/ PBS solution

486 for 210 minutes at room temperature. SARS-CoV-2 viral nucleocapsid protein (NP) was detected

487 using the anti-NP protein antibody (PA5-81794, Thermo Fisher) diluted 1:10000 in 0.1% tween-

488 20/1%BSA/PBS solution as a primary antibody, followed by detecting with an anti-rabbit

489 secondary antibody (ab6721, Abcam) at a 1:20,000 dilution. Plates were washed three times

490 between antibody solutions using 0.5% tween-20 in PBS. The plates were developed using

491 TrueBlue Peroxidase Substrate (5510-0030, Sera Care) and then scanned using Immunospot S6

492 Sentry (C.T.L Analyzers). Neutralization titers for the immunoplaque assay are defined as a 50%

493 reduction in plaque forming units relative to the untreated wells.

Assessment of binding between S protein and FXa using ELISA

495 Full-length coronavirus S protein with His tag (500 ng) (40589-V08B1, Sino Biological),

496 coronavirus S protein S1 subunit with His tag (500 ng) (40591-V08B1, Sino Biological),

497 coronavirus S protein S2 subunit with His tag (500 ng) (40070-V08B, Sino Biological), and

498 coronavirus S protein RBD with His tag (500 ng) (40592-V08B-B, Sino Biological) were used as

499 coating reagents in 96-well plates (3361, Corning). Coated plates were incubated with FXa protein

500 (1 µg/ml) for 2 hours at room temperature. FXa-HRP conjugated anti-human Fc antibody (05-

501 4220, Invitrogen) was used as a detecting antibody. Absorbance was measured at OD450 nm using

502 a Multiskan™ FC Microplate Photometer (Fisher Scientific).

Pull-down assay

504 HEK293T cells were transduced with a pCDH lentiviral vector expressing the full-length spike (S)

505 protein for 48 hours. The cells were lysed and incubated with FXa-Fc or Fc (10 µg/ml) for 3 hours,

506 then 20 µl protein A agarose resin beads (P-400-25, Invitrogen) were added and incubated

507 overnight. After incubation, the beads were washed and collected. Protein binding between FXa-

508 Fc or Fc and S protein was detected by immunoblotting using an anti-S protein antibody

509 (ab272504, Abcam).

Cleavage assay

16

511   One microgram of full-length S protein was treated with 1 µg of FXa (P8010L, NEB), furin

512   (P8077S, NEB) or TMPRSS2 (TMPRSS2-1856H, Creative BioMart) protein for 3 hours following

513   the manufacturers' instructions. Cleavage was detected using immunoblotting with an anti-S

514   protein antibody. For inhibitor assays, FXa protein was preincubated with or without 50 µg/ml

515   rivaroxaban or fondaparinux separately for 1 hour in advance at room temperature, then treated

516   with SPs and detected as above. For cleavage assays using S protein-ACE2 complex, 1 µg S

517   protein and 1 µg ACE2 were pre-incubated 1 hour prior to incubation with FXa, then treated with

518   SPs and detected as above. Of note, we used different buffer conditions for all binding assays and

519   cleavage assays.

Assessment of binding between S protein and FXa using flow cytometry

521   HEK293T cells were transduced with lentiviral vector expressing FXa for 48 hours. The cells were

522   incubated with 10 µg/ml full-length S protein for 20 minutes at room temperature. The cells were

523   then washed and incubated with an anti-S protein antibody for 20 minutes at room temperature,

524   followed by staining with a FITC-labeled secondary antibody (111-605-045, Jackson

525   ImmunoResearch). The percentage of FITC-positive cells was determined using a Fortessa X20

526   flow cytometer (BD Biosciences).

Detection of FXa binding to S protein-ACE2 complex using ELISA

528   ACE2 protein was used as a coating reagent in 96-well plates, which were incubated with 1 µg/ml

529   full-length S protein with His tag that had been pretreated with or without FXa (P8010L, NEB) for

530   2 hours at room temperature. An HRP-conjugated anti-His tag antibody (ab1187, Abcam) was

531   used as a detecting antibody. Absorbance was measured at OD450 nm using a Multiskan™ FC

532   Microplate Photometer (Fisher Scientific).

Detection of FXa binding to S protein-ACE2 complex using flow cytometry

534   HEK293T cells stably expressing ACE2 protein were incubated with full-length S protein or FXa-

535   pretreated full-length S protein for 20 minutes at room temperature. Cells were then washed and

536   incubated with an anti-S protein antibody for 20 minutes at room temperature, followed by staining

537   with an APC-labeled secondary antibody (111-005-003, Jackson ImmunoResearch). The

538   percentage of APC-positive cells was determined using a Fortessa X20 flow cytometer (BD

539   Biosciences).

In vivo infection model

6-8-week-old K18-hACE2 mice were anesthetized with ketamine (80 mg/kg)/xylazine (8 mg/kg) and intranasally infected with 5×10^3 PFU wild type SARS-CoV-2 or B.1.1.7 variant in 25 µl DMEM, followed by intranasal treatment with PBS, FXa-Fc (200 µg), or Fc (200 µg) in 25 µl DMEM. Infected mice were maintained in BCU isolator cages (Allentown, NJ, USA) in the NAU ABLS3. Mice were then treated with PBS or rivaroxaban (30 mg/kg) via gavage or fondaparinux (30 mg/kg) via intraperitoneal injection for 4 times at a frequency of every other day *(30,31)*. Body weights of mice were monitored daily. Mice were euthanized using ketamine (100 mg/kg)/xylazine (10 mg/kg) when body weights dropped below 20% of their original body weights. RNA was isolated from trachea, lung, and brain tissues to assess viral load using quantitative real-time PCR as described below. Expression of SARS-CoV-2 viral protein NP was examined using immunohistochemistry (IHC) in the trachea, lung, and brain sections from infected mice as described below. Experiments and handling of mice were conducted under federal, state, and local guidelines and with approvals from the Northern Arizona University (20-005) and City of Hope Animal Care and Use Committees.

Quantitative real-time PCR

Mouse tissues were homogenized in DMEM and RNA was isolated using a PureLink RNA isolation kit (K156002, Invitrogen). Viral copy numbers were detected using the One-Step QPCR kit (1725150, BioRad).

H&E and IHC

4-µm-thick sections were cut from paraffin blocks of lung and liver tissues from COVID-19 patients and non-COVID-19 donors. IHC staining with an anti-FXa protein antibody (PIPA529118, Invitrogen), an anti-furin antibody (ab183495, Abcam), an anti-trypsin antibody (ab200997, Abcam), or an anti-plasmin antibody (LS-C150813-1, LSBio) as a primary antibody was performed by the Pathology Shared Resource Core at City of Hope Beckman Research Institute. Stained slides were mounted and scanned for observation.

Mouse tissues isolated from experimental mice were placed in 10% neutral buffered formalin for a minimum of 72 hours. After paraffin embedding, 4-µm-thick sections were cut from the blocks. H&E staining and IHC with anti-NP protein antibody (NB100-56576, Novus) as the primary

18

569 antibody were performed by the Pathology Shared Resource Core at City of Hope Beckman

570 Research Institute. Stained slides were mounted and scanned for observation.

571 **Statistical analysis**

572 Prism software v.8 (GraphPad, CA, USA) and SAS v.9.4 (SAS Institute. NC, USA) were used to

573 perform statistical analyses. For continuous endpoints that were normally distributed or normally

574 distributed after log transformation such as MFI or copy number, Student's t test or paired t test

575 was used to compare two independent or matched groups, respectively. One-way ANOVA models

576 or generalized linear models were used to compare three or more independent groups. For data

577 with repeated measures from the same subject, linear mixed models were used to account for the

578 variance and covariance structure due to repeated measures. Survival functions were estimated

579 using the Kaplan–Meier method and compared using the two-sided log rank test. All tests were

580 two-sided. P values were adjusted for multiple comparisons using Holm's procedure. A P value of

581 0.05 or less was considered statistically significant. The p-values are represented as: * <0.05, **

582 <0.01, *** <0.001, and **** <0.0001

583

584 **Methods references**

585 1   Zang, R. *et al.* Cholesterol 25-hydroxylase suppresses SARS-CoV-2 replication by blocking
586 membrane fusion. *Proc Natl Acad Sci U S A* **117**, 32105-32113, doi:10.1073/pnas.2012197117 (2020).

587 2   Peters, R. T. *et al.* Prolonged activity of factor IX as a monomeric Fc fusion protein. *Blood* **115**,
588   2057-2064, doi:10.1182/blood-2009-08-239665 (2010).
589 3   Stone, N. E. *et al.* Stenoparib, an Inhibitor of Cellular Poly(ADP-Ribose) Polymerase, Blocks
590   Replication of the SARS-CoV-2 and HCoV-NL63 Human Coronaviruses In Vitro. *mBio* **12**,
591   doi:10.1128/mBio.03495-20 (2021).
592 4   Case, J. B., Bailey, A. L., Kim, A. S., Chen, R. E. & Diamond, M. S. Growth, detection,
593   quantification, and inactivation of SARS-CoV-2. *Virology* **548**, 39-48,
594   doi:10.1016/j.virol.2020.05.015 (2020).

595

596

597 **ACKNOWLEDGMENTS**

600   Lymphoma Society (1364-19 to J. Yu), The California Institute for Regenerative Medicine

601   (DISC2COVID19-11947 to J. Yu), and The Flinn Foundation grant 2304 (PK and BB) and

602   Arizona Board of Regents TRIF award (PK).

603

604   **AUTHORS' CONTRIBUTIONS**

605   J. Yu, M.A. Caligiuri, and W. Dong conceived and designed the project. J. Yu, M.A. Caligiuri, W.

606   Dong, J. Wang, L. Tian, H. Mead, S. Jaramillo, E. Settles, P. Keim and B. Barker designed and

607   supervised experiments conducted in the laboratories. Dong, J. Wang, L. Tian, J. Zhang, A. Li,

608   performed experiments and/or data analyses. R. Zumwalt provided the COVID-19 patient samples.

609   S. Whelan provided VSV-SARS-CoV-2. W. Dong, L. Tian, E. Settles, P. Keim, B. Barker, J. Yu,

610   and M.A. Caligiuri wrote, reviewed and/or revised the paper. All authors discussed the results and

611   commented on the manuscript.

612

613   **DECLARATION OF INTERESTS**

614   No author has a direct conflict of interest relevant to this research to declare.

615

616

617

618

619

620

621

622

623

624

625

626

627

628 **Figures and Figure legends**
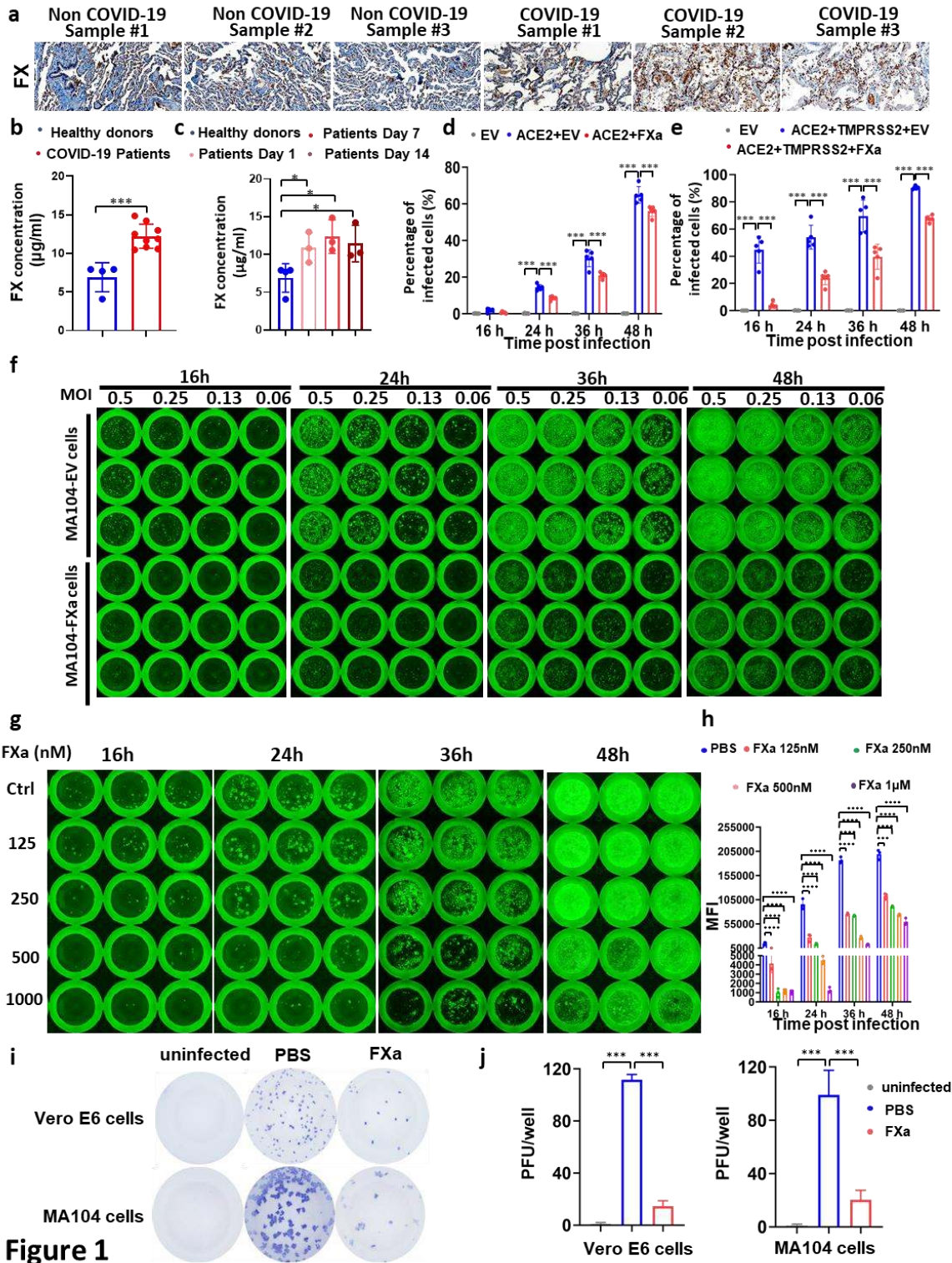
Figure 1

629

630 **Fig. 1. FXa inhibits wild-type SARS-CoV-2 infection by targeting viral particles.** (**a and b**)

631 FX protein levels in lungs (a) or serum (b) of COVID-19 patients vs. non-COVID-19 donors, using

632 IHC (a) and ELISA (b), respectively. (**c**) FX concentrations in serum of COVID-19 patients as

633 shown post diagnosis of infection were measured by ELISA. (**d and e**) HEK293T cells co-

634 transfected with ACE2 and FXa or an EV in the absence (d) or presence (e) of TMPRSS2 were

635 infected by VSV-SARS-CoV-2, and quantified by flow cytometry at 16, 24, 36, and 48 hpi. (**f**)

636 MA104 cells transduced with FXa (MA104-FXa) or EV (MA104-EV) were infected by VSV-

637 SARS-CoV-2 and imaged at 16, 24, 36, and 48 hpi by fluorescence microscopy. (**g and h**) VSV-

638 SARS-CoV-2 was preincubated with FXa at indicated concentrations 1 hour before infection. Cells

639 were imaged at 16, 24, 36, and 48 hpi by fluorescence microscopy (g) and the corresponding

640 infectivity was measured by flow cytometry (h). (**i and j**). MA104 and Vero E6 cells were infected

641 with live wild-type SARS-CoV-2. At 24 hpi, infectivity was measured by immune-plaque assay

642 (i). (j) The summary data of (i). Experiments in i are representative of two independent experiments

643 with similar data, and the other data are representative of at least three independent experiments.

644 For all panels, error bars indicate standard deviation (SD), and statistical analyses were performed

645 by Student's t tests (b-e) and linear mixed model (h). *P ≤ 0.05; **P ≤ 0.01; ***P ≤ 0.001; ****P ≤
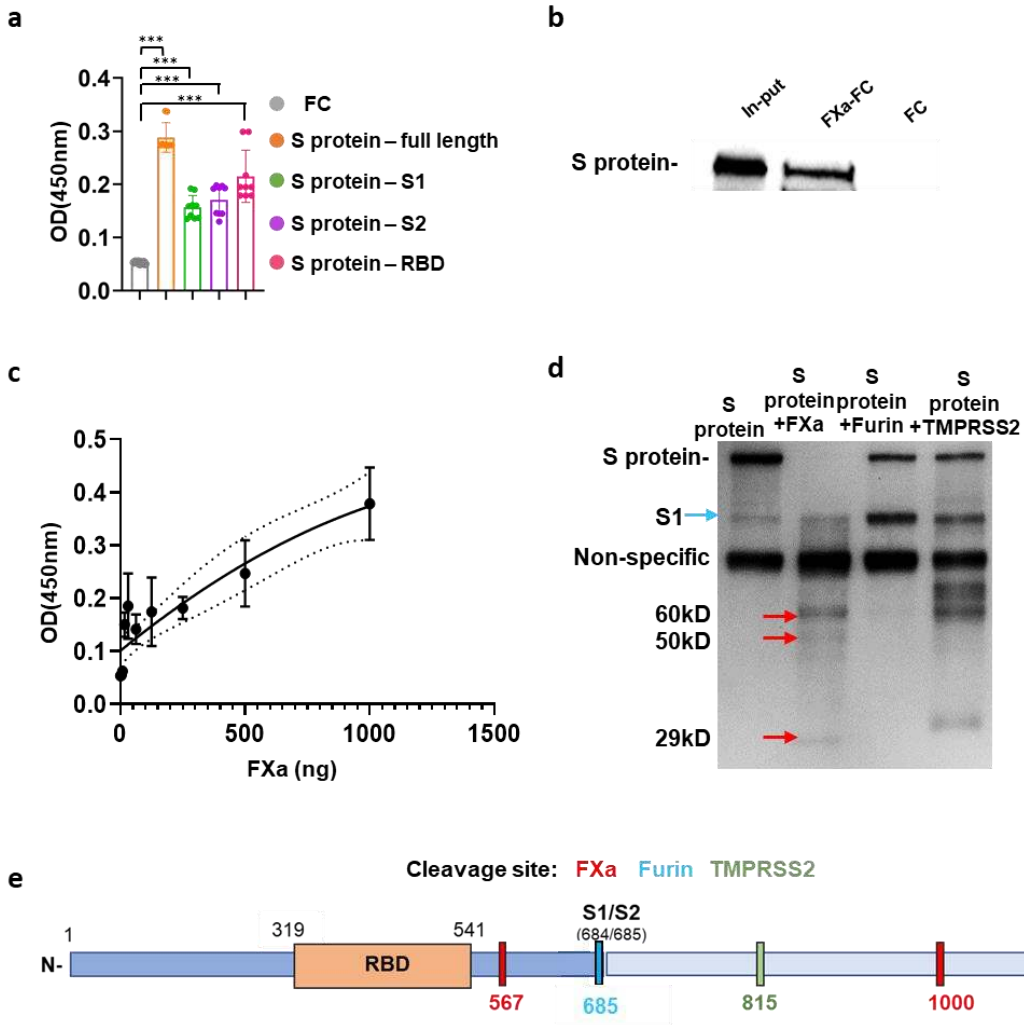
646 0.0001; n.s, not significant.

647

648

649

22

Figure 2

650

651

Fig. 2. FXa suppresses viral entry by binding to and cleaving the SARS-CoV-2 S protein. (**a**) The binding affinity of FXa with full-length wild-type S protein, subunit S1, subunit S2, and RBD was quantified by ELISA. (**b and c**) The interaction between FXa protein and full-length S protein was examined by pull-down assay (b). The binding affinity at indicated concentrations of FXa was measured by ELISA (c). (**d**) The cleavage of S protein by furin, TMPRSS2, and FXa was analyzed by immunoblotting. (**e**). Schema of the cleavage sites for furin, TMPRSS2 and FXa on the full-length S protein. (**f**) 293 T cells were co-transfected with a S protein expression plasmid and various amounts of an FXa expression plasmid. S protein cleavage by FXa inside of cells was analyzed by immunoblotting. All data are representative of at least three independent experiments. Experiments in b and d are representative of three independent experiments with similar data. For

23

662   all panels, error bars indicate SD, and statistical analyses were performed by one-way ANOVA

663   models. ***P ≤ 0.001.
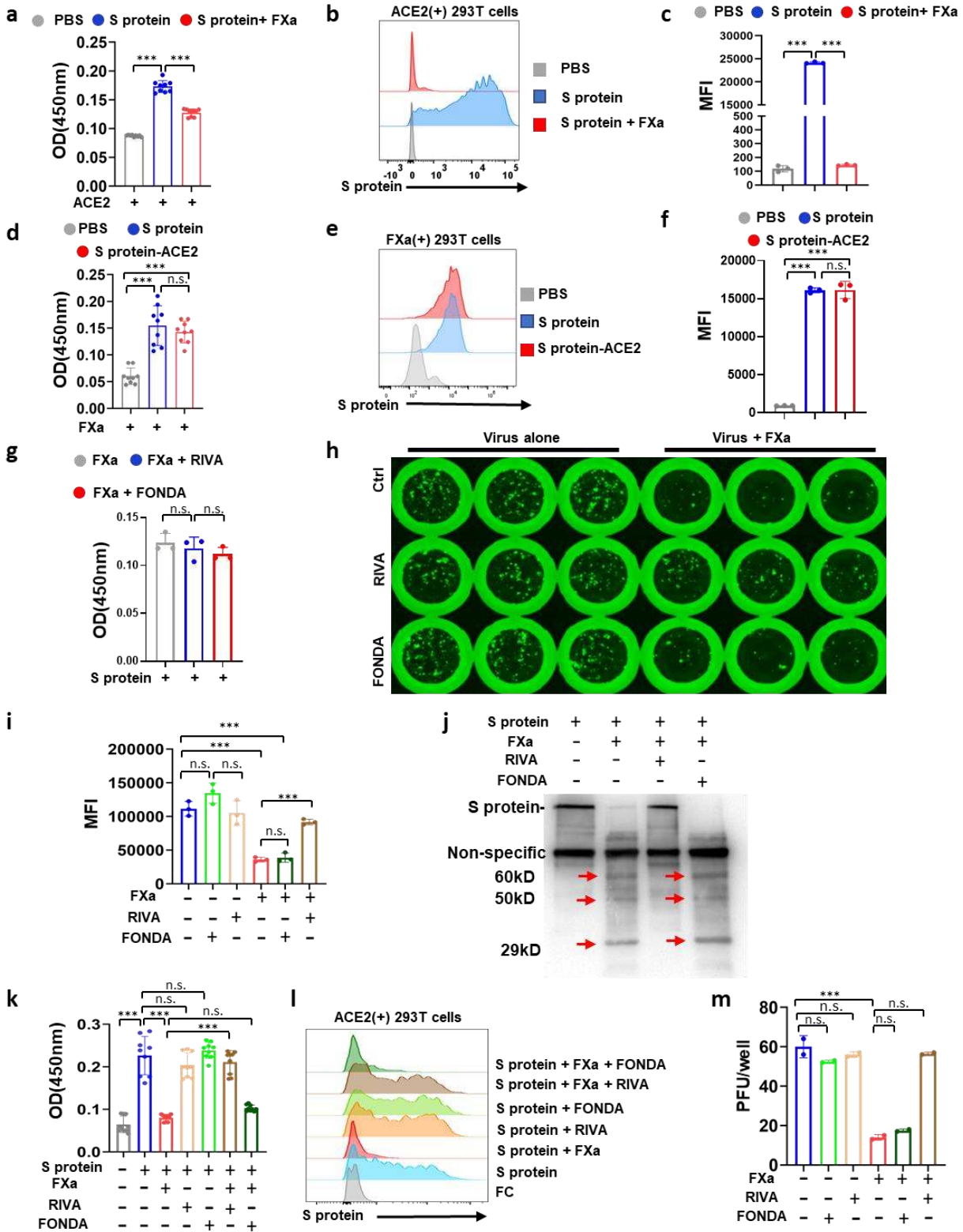
664

Figure 3

665

666

25

667   **Fig. 3. FXa cleavage blocks the binding between S protein and ACE2.** (**a**) The binding between

668   ACE2 with S protein or FXa-pretreated S protein was measured by ELISA. (**b and c**) The binding

669   between S protein or FXa-pretreated S protein and ACE2 expressed on 293T cells was measured

670   by flow cytometry (b and c, summary data). (**d**) The binding of FXa with S protein, S protein-

671   ACE2 complex, or PBS control, assessed by ELISA. (**e** and **f**) The binding between the S protein

672   or the S protein-ACE2 complex with FXa expressed on 293T cells. PBS served as control for S

673   protein and S protein-ACE2 complex. (**g**) The effect of RIVA or FONDA on the binding of FXa

674   with S protein was measured by ELISA. (**h and i**) The infectivity of FXa-pretreated vs. untreated

675   VSV-SARS-CoV-2 in MA104 cells in the presence or absence of RIVA or FONDA was examined

676   with fluorescent microscopy (h) and flow cytometry (i). (**j**) S protein cleavage by FXa in the

677   presence or absence of RIVA or FONDA was examined by immunoblot. (**k and l**) FXa pretreated

678   with or without RIVA or FONDA was incubated with S protein, followed by assessing the binding

679   capability of these S proteins with ACE2 coated on a plate (j) or expressed on 293T cells (l). (**m**)

680   The infectivity of FXa-pretreated vs. untreated live SARS-CoV-2 in MA104 cells in the presence

681   or absence of RIVA or FONDA was examined using an immune-plaque assay. All data are

682   representative of at least three independent experiments. Experiments in h and j are representative

683   of three independent experiments with similar data. For all panels, error bars indicate SD, and

684   statistical analyses were performed by one-way ANOVA models. ***$P \leq 0.001$; n.s, not
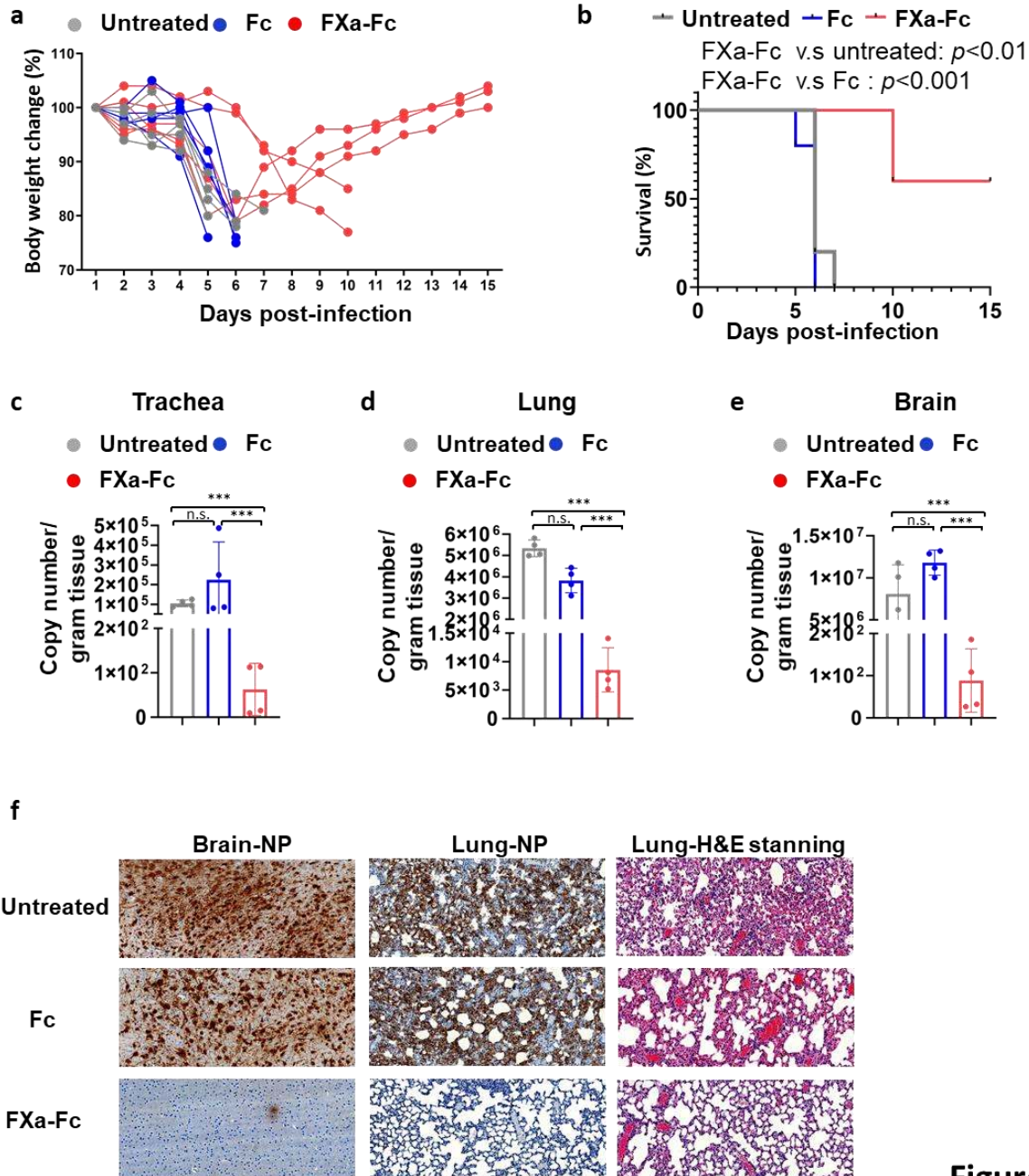
685   significant.

686

Figure 4

687

688

Fig. 4. The effect of FXa protein on WT SARS-CoV-2 infection in a K18-hACE2 mouse model of COVID-19. (**a and b**) Body weight (a) and survival (b) of mice infected with 3×10^5 PFU SARS-CoV-2 WTstrain and treated with or without FXa-Fc fusion protein. Fc-protein was used as control. (**c-e**) Viral load in the tracheas (c), lungs (d), and brains (e) of mice treated with or without FXa-Fc fusion protein or Fc control was assessed by Q-PCR. (**f**) The presence of SARS-

27

694 CoV-2 was determined using IHC staining with an antibody against viral nucleocapsid protein
695 (NP) in the brain and lung of mice treated with FXa-Fc or Fc-protein. Pathological analysis of the
696 lung of mice treated with or without FXa-Fc or Fc-protein as performed by H&E staining. For all
697 panels, error bars indicate SD, and statistical analyses were performed by one-way ANOVA
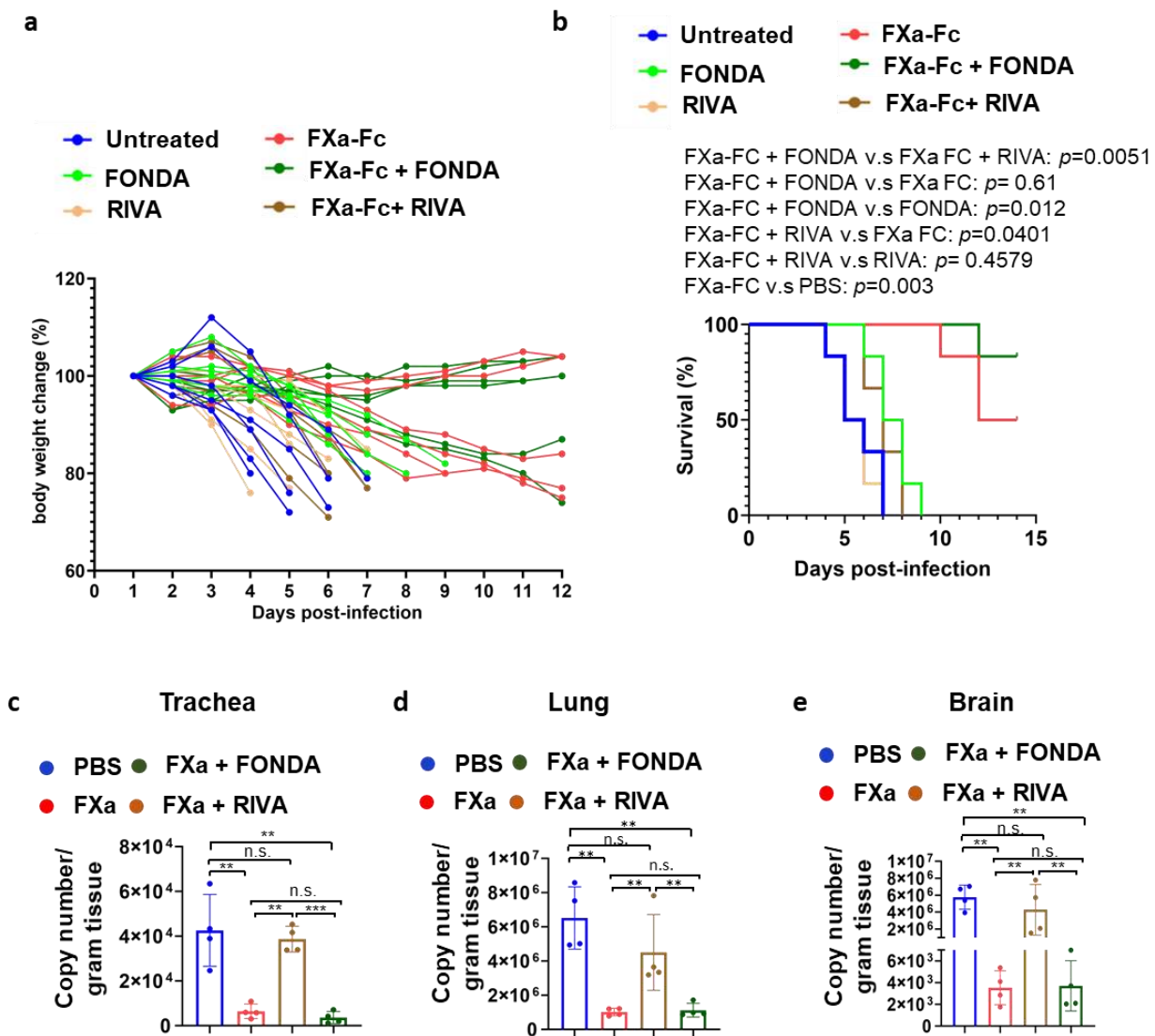698 models (c, d, e) and log-rank test (b). ***$P \leq 0.001$; n.s, not significant.

699

700

701

Figure 5

702

703

Fig. 5. The effect of the direct FXa inhibitor RIVA and the indirect inhibitor FONDA on FXa-mediated protection of K18-hACE2 mice from WT SARS-CoV-2 infection. (**a and b**) Body weight (a) and survival (b) of mice infected with 3×10^5 PFU SARS-CoV-2 (WT-1) and treated with or without FXa-Fc in the presence or absence of RIVA or FONDA. (**c-e**) Viral load in the trachea (c), lung (d), and brain (e) of mice treated with or without FXa-Fc in the presence or absence of RIVA or FONDA was assessed by Q-PCR. For all panels, error bars indicate SD, and statistical analyses were performed by one-way ANOVA models (c, d, e) and log-rank test (b). **$P \leq 0.01$; ***$P \leq 0.001$; n.s, not significant.
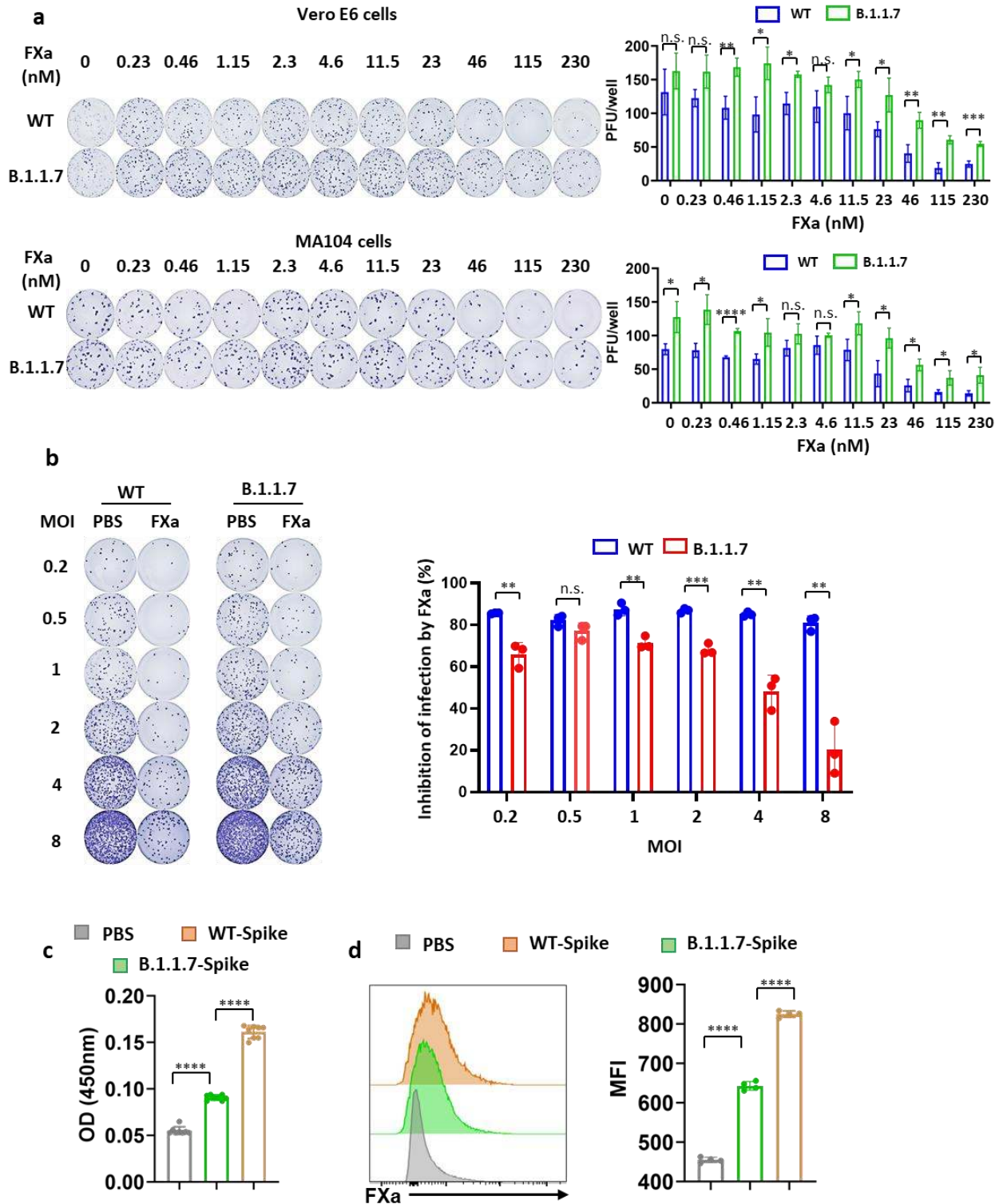
Figure 6

714   **Fig. 6. FXa blocks the B.1.1.7 variant infection less efficiently compared to the WT SARS-**

715   **CoV-2 due to different binding affinity to the corresponding S protein.** (**a**) MA104 and Vero

716   E6 cells were infected with either the live wild-type or the B.1.1.7 variant of SARS-CoV-2

717   pretreated with different doses of FXa. At 24 hpi, infectivity was measured by immune-plaque

718   assay. The representative infection and the summary data are presented at the left and right,

719   respectively. (**b**) MA104 and Vero E6 cells were infected with live wild-type or the B.1.1.7 SARS-

720   CoV-2 variant pretreated with FXa at different MOIs. At 24 hpi, infectivity was measured by

721   immune-plaque assay (left panel) and the infection inhibition ratio induced by FXa at different

722   MOIs are summarized (right panel). (**c**) The binding FXa with wild-type S protein or B.1.1.7

723   variant S protein, assessed by ELISA. (**d**) The binding between wild-type S protein or B.1.1.7

724   variant S protein with FXa expressed on 293T cells, assessed by flow cytometry. PBS serves as

725   control. For all panels, error bars indicate SD, and statistical analyses were performed by one-way

726   ANOVA models. $*P \leq 0.05$; $**P \leq 0.01$; $***P \leq 0.001$; $****P \leq 0.0001$; n.s, not significant.
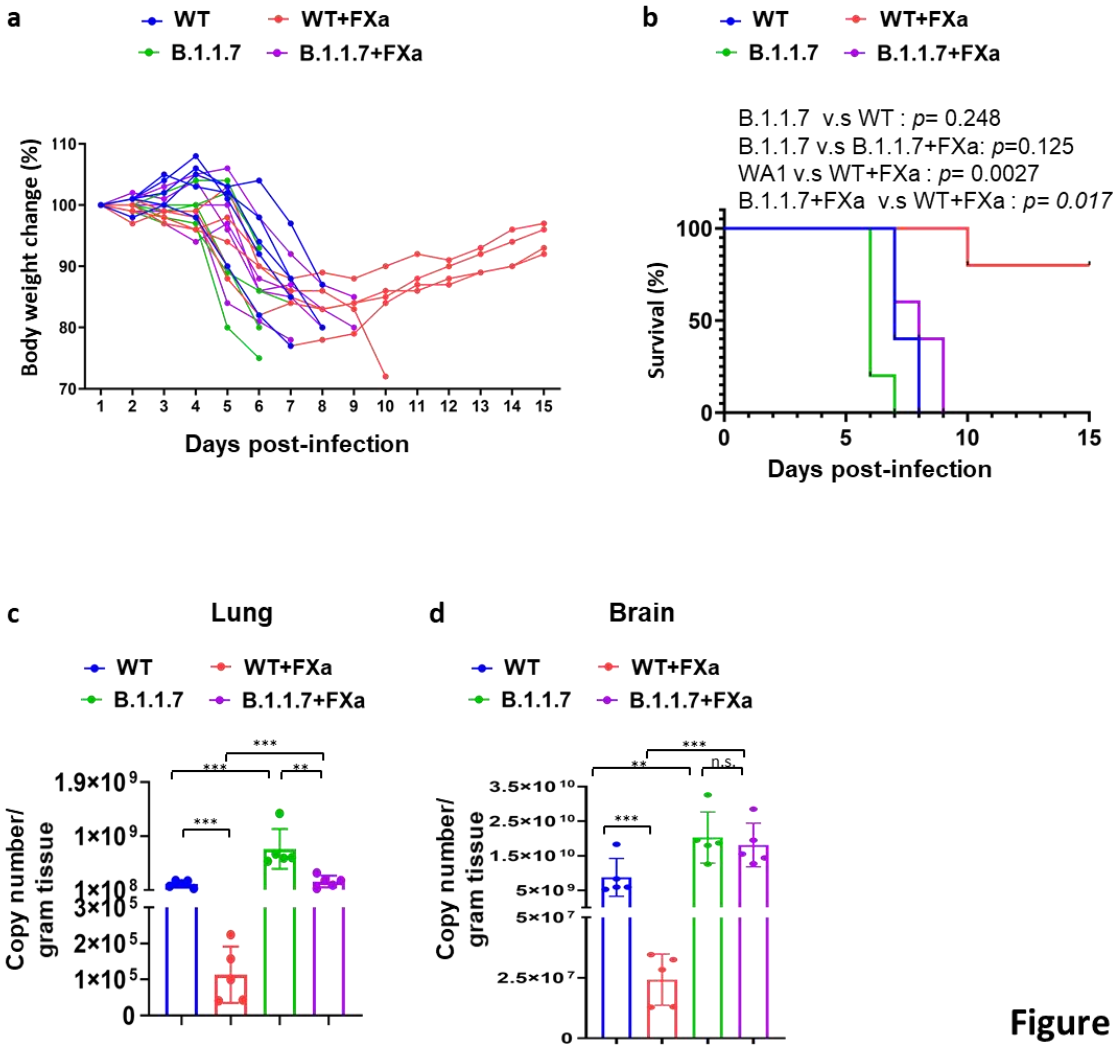
727

31

Figure 7

Fig. 7. The effect of FXa protein on live B.1.1.7 variant infection in in a lethal humanized hACE2 mouse model of SARS-CoV-2 infection. (**a and b**) Body weight (a) and survival (b) of mice infected with 3×10^5 PFU wild-type SARS-CoV-2 or B.1.1.7 variant and treated with or without FXa-Fc fusion protein. (**c and d**) Viral load in the lung (c) and brain (d) of mice treated with or without FXa-Fc fusion protein was assessed by quantitative PCR. For all panels, error bars indicate SD, and statistical analyses were performed by one-way ANOVA models (c and d) and log-rank test (b). ***$P \le 0.001$; n.s, not significant.